THE JOURNAL OF PHYSICAL CHEMISTRY A
A JOURNAL OF THE AMERICAN CHEMICAL SOCIETY

pubs.acs.org/JPCA Article

Five Birds with One Stone: Photoelectron Photoion Coincidence Unveils Rich Phthalide Pyrolysis Chemistry

Published as part of The Journal of Physical Chemistry virtual special issue "Cheuk-Yiu Ng Festschrift".

Jordy Bouwman,* Helgi R. Hrodmarsson, G. Barney Ellison, Andras Bodi, and Patrick Hemberger

Cite This: https://dx.doi.org/10.1021/acs.jpca.1c00149 Read Online

ABSTRACT: Phthalide pyrolysis has been assumed to be a clean fulvenallene source. We show that this is only true at low temperatures, and the C_7H_6 isomers 1-, 2-, and 5-ethynylcyclopentadiene are also formed at high pyrolysis temperatures. Photoion mass-selected threshold photoelectron spectra are analyzed with the help of (time-dependent) density functional theory, (TD-)DFT, and equation-of-motion ionization potential coupled cluster, EOM-IP-CCSD, calculations, as well as Franck−Condon simulations of partly overlapping bands, to determine ionization energies. The fulvenallene ionization energy is confirmed at 8.23 ± 0.01 eV, and the ionization energies of 1-, 2 and 5-ethynylcyclopentadiene are newly determined at 8.27 ± 0.01, 8.49 ± 0.01 and 8.76 ± 0.02 eV, respectively. Excited state features in the photoelectron spectrum, in particular the $\tilde{A}^+\,^2A'$ band of 1-ethynylcyclopentadiene, are shown to be practical to isomer-selectively detect species when the ground-state band is congested. At high pyrolysis temperatures, the C_7H_6 isomers may lose a hydrogen atom and yield the fulvenallenyl radical. Its ionization energy is confirmed at 8.20 ± 0.01 eV. The vibrational fingerprint of the first triplet fulvenallenyl cation state is also revealed and yields an ionization energy of 8.33 ± 0.02 eV. Further triplet cation states are identified and modeled in the 10−11 eV range. A reaction mechanism is proposed based on potential energy surface calculations. Based on a simplified reactor model, we show that the C_7H_6 isomer distribution is far from thermal equilibrium in the reactor, presumably because irreversible H loss competes efficiently with isomerization.

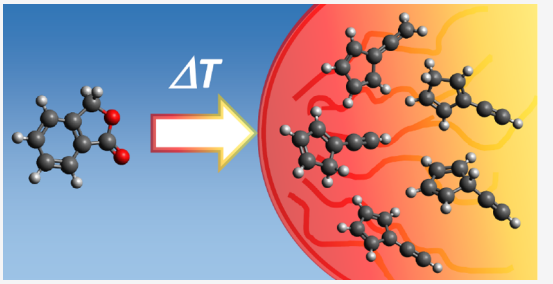

INTRODUCTION

Polycyclic aromatic hydrocarbons (PAHs) are emitted into the atmosphere on a large scale as byproducts of natural and anthropogenic combustion,[1] and have adverse health effects.[2] Looking beyond the bio- and anthroposphere, PAHs are also abundant in the interstellar medium (ISM) as evidenced by their ubiquitous IR emission bands.[3−5] In the ISM, PAHs are believed to be formed in outflows of carbon-rich stars by processes reminiscent of those in combustion.[6,7] PAHs containing pentagonal structures are also widespread and may play an important role in the formation of curved PAHs and perhaps ultimately fullerenes.[8−12] It is thus critical to understand the reactivity and spectroscopy of such pentagon-bearing hydrocarbons.

Hydrocarbons of C_7H_6 composition are commonly formed in combustion experiments.[13] There are four cyclopentadiene-based C_7H_6 isomers—fulvenallene (**FA**), 1-ethynylcyclopentadiene (**1ECP**), 2-ethynylcyclopentadiene (**2ECP**), and 5-ethynylcyclopentadiene (**5ECP**) (see Figure 1)—and of these structures, **FA** is the most stable one.[14] Fulvenallene is formed in the thermal decomposition of benzyl radicals.[15,16] All four cyclopentadiene-based C_7H_6 isomers yield the resonance-stabilized fulvenallenyl radical (**FArad**)—a PAH and soot precursor—directly via H loss.[17] This motivated experimental and computational studies of these species in the past.

In a He I photoelectron spectroscopic study, Müller et al.[18] reported the ionization energy of **FA** as 8.29 eV to the $\tilde{X}^+\,^2A_2$ ground state of the cation. They pyrolytically induced the isomerization of 1,2-diethynylcyclopropane, which had previously been shown to yield bicyclo[3.2.0]hepta-l,4,6-triene, **FA**, and **ECP** isomers together with heptafulvalene, depending on the pyrolysis conditions.[19] Early experiments on the thermolysis of the lactone phthalide (2-benzofuran-1(3*H*)-one, $C_8H_6O_2$, see Figure 1 for the structure) revealed that **FA** and **ECP** isomers are formed, among other minor breakdown products.[20,21] Botter et al.[22] pyrolyzed phthalide, isolated and stabilized the product using tetracyanoethylene, and recorded a photoelectron spectrum yielding 8.22 eV as the **FA** ionization energy. The photoelectron spectrum also showed two

Received: January 7, 2021
Revised: February 4, 2021

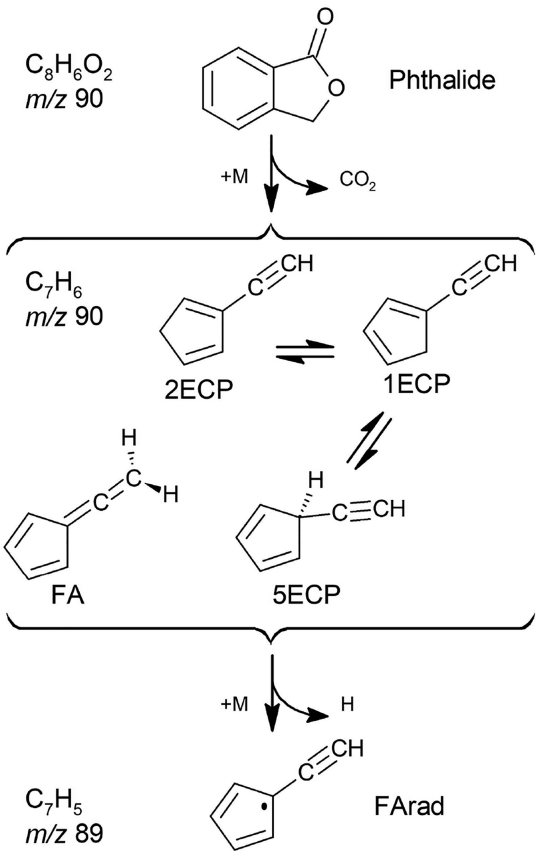

Figure 1. Phthalide pyrolysis mechanism with the species relevant to this work.

unresolved bands at 9.14 and 10.15 eV, which were attributed to electronically excited cation states of $^2B_1$ and $^2B_2$ symmetry, respectively. The notation assumes *yz* to be the principal plane in C_{2v} symmetry, which we will use herein, too. Three decades later, Steinbauer et al.[23] studied the photoelectron spectroscopy of **FA** and **FArad**. In their work, phthalide was pyrolyzed in a SiC microreactor and the threshold photoelectron spectra (TPES) of the products were recorded using synchrotron-based imaging photoelectron photoion coincidence (iPEPICO) spectroscopy. A strong resonance was found at 8.22 eV in photoion mass-selected (ms-)TPES of *m*/*z* 90 and ascribed to ionization of **FA** to the $^2A_2$ ground state of the ion. The comparably clean C_7H_6 spectrum is intriguing in light of the potential energy surface (PES) study by Kvaskoff et al.,[24] which showed that the various isomers are connected by relatively low-lying open-shell singlet (OSS) biradical species, making it difficult to prepare one isomer selectively in a hot environment. Steinbauer et al.[23] also reported an ionization resonance at 8.19 eV in the *m*/*z* 89 ms-TPES and attributed this to ionization of **FArad** to its $\tilde{X}^+\,^1A_1$ ground state.

Li et al.[25] attempted to determine the isomeric composition of C_7H_6 species detected in combustion and flame studies. Hansen et al.[13] found that C_7H_6 was formed in a fuel-rich cyclopentene flame by synchrotron-based photoionization mass spectrometry. With a lack of experimental ionization energies (IEs) for most C_7H_6 isomers, they computed adiabatic IEs to assign the photoionization signal. They concluded that the measured ionization threshold at 8.23 eV can be attributed to either **FA** or **1ECP**, and because of their somewhat higher computed ionization energy, it was concluded that **2ECP** and **5ECP** do not contribute to the *m*/*z* 90 signal. Evidently, the differences in the published experimental IEs for **FA** and the proximity of the computed ionization thresholds of the isomers make it hard to base the isomer-specific assignment of C_7H_6 on the ionization energy alone.

Because of spectral congestion, the detailed and well-resolved characterization of the TPES of the C_7H_6 isomers and the resonance stabilized $C_7H_5^\bullet$ radical in general and the identification of excited-state spectral signatures in particular are crucial to identify these species in the gas phase. In the past, we have shown that this approach works well for complex chemical systems where many isomers may be formed.[26] In this work, we revisit the photoelectron spectroscopy of the C_7H_6 isomers and of **FArad**, formed upon pyrolysis of phthalide, by combining double imaging photoelectron photoion coincidence (i^2PEPICO) experiments with quantum chemical computations and resolve contradicting assignments in the literature. Pyrolysis time-of-flight (TOF) mass spectra and photoion mass-selected threshold photoelectron (ms-TPE) spectra are recorded for various pyrolysis temperatures. Isomeric products are assigned by comparing the measured TPE spectra to Franck−Condon simulations. The C_7H_6 potential energy surface is explored, and a simplified reactor model is presented to explain the observed products and point out the remaining open questions.

METHODS

Experimental Section. The experiments have been performed using a pyrolysis microreactor connected to the double imaging photoelectron photoion coincidence endstation (CRF-PEPICO) at the vacuum ultraviolet (VUV) beamline of the Swiss Light Source. Details about the beamline,[27,28] the endstation,[29] and the Chen-type pyrolysis reactor[30] can be found elsewhere, and only a brief summary of the experiment is provided here.

The phthalide sample (98%, Sigma−Aldrich) was put in a $^1/_4$ in. tube with a 100 μm pinhole (Lennox Laser) between a small aluminum pellet and glass wool. The tube was mounted in a temperature-controlled copper block in the source chamber and heated to 343 K to ensure sufficient vapor pressure of the sample. The pyrolysis microreactor—a ca. 2 cm long and a 1 mm internal diameter SiC tube resistively heated using a DC power supply—was mounted in front of the pinhole. The phthalide vapor was picked up by a 20 sccm flow of argon. The gas passed through the tube and expanded into the hot pyrolysis microreactor through the pinhole at the end. The temperature is estimated from the heating power based on prior calibration measurements. There is a large uncertainty (±100 K) in the absolute temperature inside the reactor that is derived from the heating power, but the relative temperatures between the various measurements reported here are accurate.

The surviving phthalide precursor and the pyrolysis products exit the microreactor with the argon flow into the source chamber, which is kept at a pressure of 6×10^{-5} mbar by one cryogenic and two turbomolecular pumps. The resulting molecular beam is skimmed using a 2 mm diameter skimmer from Beam Dynamics, before it enters the detection chamber, which is kept at a background pressure of 2×10^{-6} mbar by a turbomolecular pump. The synchrotron radiation is generated using a bending magnet, dispersed with a 150 grooves/mm blazed grating, and passed through a differentially pumped gas filter containing a mix of krypton, argon, and neon to remove

https://dx.doi.org/10.1021/acs.jpca.1c00149
J. Phys. Chem. A XXXX, XXX, XXX−XXX

light resulting from higher grating orders. The light is focused onto a 200 μm exit slit, located before the detection chamber, resulting in a resolution of 8 meV at a flux of ca. 10^{12} photons/s in the studied energy range.

The molecular and the VUV beams intersect in the detection chamber. Ions and electrons formed by photoionization of species entrained in the molecular beam are extracted in opposite directions by a constant, 218 V cm^{-1} electric field and are detected in delayed coincidence by Roentdek delay line detectors.[29] The electrons are velocity map imaged to measure their kinetic energy. Thanks to their negligible flight time, they also provide the start time for the time-of-flight (TOF) measurement of the coincident ions. The photoionization mass spectrum is constructed by plotting the ion counts as a function of TOF for *all* electrons, i.e., regardless of the electron energy. To plot the ms-TPES, only electrons imaged onto the center of the detector are selected for the TOF start signal. The center signal is still contaminated by nonthreshold electrons that happen to have no off-axis momentum component. This hot electron contamination was approximated based on a ring area around the center spot and subtracted from the center signal to obtain the threshold photoionization signal.[31]

Computational Methods. The experimental data are supported by computational studies using Gaussian 16 and Q-Chem 4.3.[32,33] To identify the isomers that may ionize at a given photon energy, adiabatic ionization energies were computed using the CBS-QB3 composite method first.[34] Vertical ionization energies were also calculated at the EOM-IP-CCSD/cc-pVTZ//B3LYP/6-311++G(d,p) level of theory.[35] CBS-QB3 adiabatic ionization energies are reported with and EOM-IP results are reported without zero-point corrections. Franck−Condon simulations can be used to establish isomer-specific vibronic fingerprints unambiguously, even when they arise in the midst of broader progressions in a mix of isomers. We carried out geometry optimizations and frequency calculations using density function theory (DFT) for the ground neutral and cation states and time-dependent (TD-)DFT calculations for selected excited states to assign the ms-TPES features in an isomer-selective manner. Franck−Condon factors were calculated in the double harmonic approximation including the Duschinsky rotations using ezSpectrum.[36] The simulated stick spectrum was convoluted with a Gaussian function with a full width at half-maximum (fwhm) of 160 cm^{-1} to account for the rotational broadening and the resolution of the experiment and then compared with the recorded ms-TPES.

To rationalize the pyrolysis and isomerization reactions, we explored the potential energy surface (PES) at the B3LYP/6-311++G(d,p) level of theory using constrained optimizations and internal coordinate scans. On the basis of CBS-QB3 energetics, we also discuss a simplified reactor model to account for the observed product distributions.

RESULTS AND DISCUSSION

Mass Spectrometry. Temperature-dependent pyrolysis mass spectra show that phthalide (m/z 134) pyrolysis sets in at 1030 K and leads to C_7H_6 formation at m/z 90 (Figure 2):

$$C_8H_6O_2 \rightarrow C_7H_6 + CO_2$$

As shown by Steinbauer et al.[23] and evidenced by the strong m/z 105 peak in the electron ionization mass spectrum of

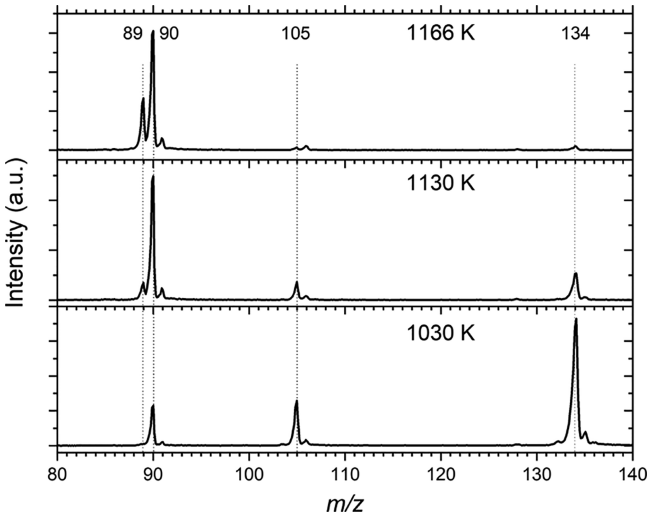

Figure 2. Phthalide pyrolysis mass spectra recorded at representative temperatures at a photon energy of 10 eV.

phthalide,[37] dissociative photoionization (DPI) of phthalide readily yields m/z 105 via:

$$C_8H_6O_2 \xrightarrow{h\nu} C_7H_5O^+ + HCO^\bullet + e^-$$

Dissociative photoionization is enhanced in pyrolysis by the incomplete vibrational cooling of the precursor in the molecular beam.[38] At a reactor temperature of 1130 K, the parent molecule gets depleted nearly completely, as is evidenced by the simultaneously weakened m/z 105 and 134 peaks. As the temperature is increased further to 1166 K, a signal grows in at m/z 89, which is ascribed to hydrogen loss from the primary pyrolysis product at m/z 90:

$$C_7H_6 \rightarrow C_7H_5^\bullet + H^\bullet$$

Identification of the *m/z* 90 Products. Mass-selected threshold photoelectron spectra were recorded at various reactor temperatures to reveal if there is a change in the isomeric composition of the pyrolysis products. Overview TPE spectra are available in the Supporting Information (Figure S1) and we focus on the energy ranges with resolved vibronic structure here. First, the ms-TPE spectra recorded at two temperatures, 1030 and 1166 K, are shown in Figure 3 in the 8.1−9.0 eV photon energy range. There is a clear dependence of the photoelectron spectrum on the pyrolysis temperature. In the low-temperature spectrum, a single sharp resonance is seen at 8.22 eV followed by a series of weaker vibronic resonances at higher energy. This sharp resonance was previously detected at 8.22 eV and ascribed to **FA**.[23] When the temperature is increased to 1166 K, an additional, strong resonance appears at 8.26 eV, and further subtle changes are apparent in the shape of the TPES, particularly at 8.44, 8.48, 8.57, 8.75, and 8.92 eV where new, weak resonances are seen.

CBS-QB3 calculations have been performed to establish the adiabatic ionization energies (IEs) of the C_7H_6 isomers (Table 1). Based on these calculations, **FA** or **1ECP** could both be responsible for the strong origin transition observed in the spectrum at 8.22 eV. It is only with the help of Franck−Condon simulations that we can establish ionization to the ground $^2A_2$ state of **FA** as the main carrier of the m/z 90 spectrum (purple simulation in Figure 3), because of the strong resonance at ca. 8.4 eV. This assignment confirms that

https://dx.doi.org/10.1021/acs.jpca.1c00149
J. Phys. Chem. A XXXX, XXX, XXX−XXX

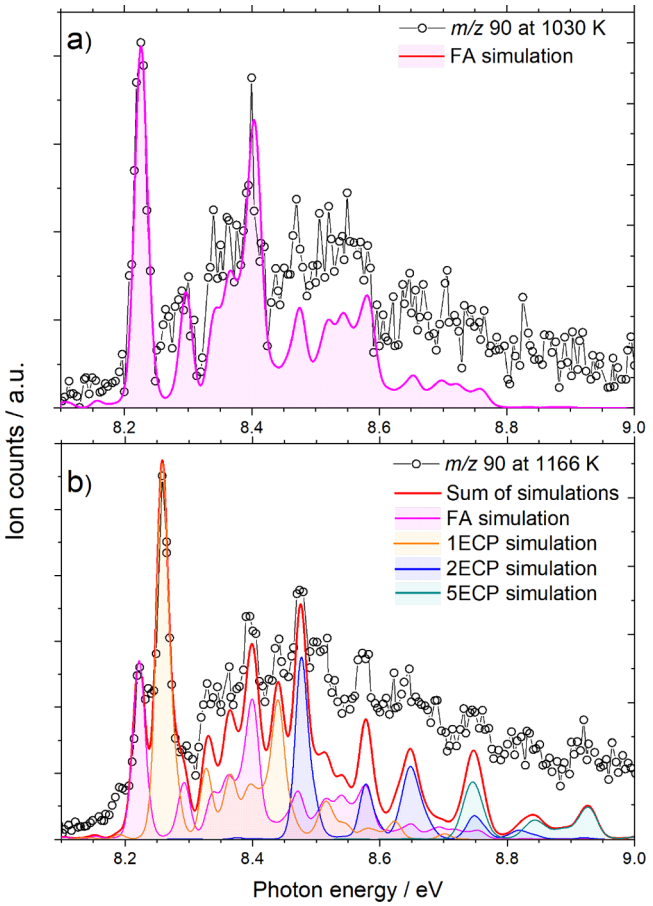

Figure 3. Mass-selected threshold photoelectron spectrum for m/z 90. (*a*) Phthalide was seeded in argon and pyrolyzed at 1030 K. The simulated TPES of fulvenallene (**FA**) is also shown. (*b*) Pyrolysis temperature raised to 1166 K. This simulation consists of the computed TPE spectra of **FA**, 1-ethynylcyclopentadiene (**1ECP**), 2-ethynylcyclopentadiene (**2ECP**), and 5-ethynylcyclopentadiene (**5ECP**). The sum is plotted in red for comparison with the experimental trace (black).

of Steinbauer et al.[23] CBS-QB3 predicts an ionization energy of 8.25 eV for **1ECP**, which makes this isomer a prime candidate to explain the changing vibrational structure as a function of pyrolysis temperature. The simulated TPE spectrum of **1ECP** is shown in Figure 3b, and it is evident that the strongest resonance in the 1166 K spectrum at 8.28 eV can be attributed to this isomer. The agreement between the experimental and the Franck−Condon simulated spectrum is further improved by the inclusion of a third isomer, **2ECP**, which has a calculated IE of 8.49 eV. This is mainly due to the reproduction of the weak, but clearly visible peaks at 8.48 and 8.57 eV. The fourth C_7H_6 isomer, **5ECP**, has a calculated IP of 8.71 eV and is found to account for the weak resonances above 8.7 eV. Due to the mobility of the hydrogens in cyclopentadienyl ring moiety, sigmatropic rearrangements are likely to occur and are responsible for the observation of all three **ECP** isomers, as was shown previously.[40,41]

A spectrum composed of the sum of the four contributing isomers is shown in red in Figure 3 and agrees well with all main resonances. The experimental ionization energies are obtained by shifting the onset of the Franck−Condon simulations to best fit the recorded ms-TPE and are listed in Table 1. To our knowledge, this spectral analysis yields the first experimentally determined ionization energies for **1ECP**, **2ECP**, and **5ECP**. Note that the values listed in Table 1 have been corrected for the 0.01 eV Stark shift in the extraction field, while the spectra shown in this manuscript have not been corrected.

The high energy part of the m/z 90 ms-TPE spectrum recorded at 1166 K and stretching from 9.8 to 10.9 eV is shown in Figure 4. This part of the spectrum reveals vibronic structure that results from ionization to an excited state of one of the identified products (*vide supra*). Contributions by excited states of **FA** can be ruled out, as no resolved substructure is observed in the 1030 K TPE spectrum, fully attributed to **FA** (Figure S1). Moreover, the ionization resonance to the ground state of **1ECP** has a much stronger ground state transition than those of **2ECP** and **5ECP**, which makes it more likely that **1ECP** features dominate the high-energy part of the spectrum, as well. EOM-IP-CCSD/cc-pVTZ calculations predict the vertical ionization energies to the first excited states of **1ECP** and **2ECP** at 10.47 and 10.34 eV, respectively. EOM-IP-CCSD geometry optimizations have failed to converge but suggest that the adiabatic ionization energies are at least ca. 0.1 eV lower. This was confirmed using the TD-DFT optimized geometry of the $\tilde{A}^+\,^2A'$ state of **1ECP**. Furthermore, vibrational analysis of the TD-DFT optimized geometries of the first excited states of **1ECP** and **2ECP** allowed for Franck−Condon simulation of this band. As shown in Figure 4, the simulated $\tilde{A}^+\,^2A'$ **1ECP** band matches the measured vibronic resonances very well. The Franck−Condon simulation of the $\tilde{A}^+\,^2A''$ **2ECP** band appears to account for the red wing of the main transition, but this assignment is less certain. Aside from these states, vertical excitations are predicted by EOM-IP-CCSD at 9.28 and 10.23 eV to the $\tilde{A}^+\,^2B_1$ and $\tilde{B}^+\,^2B_2$ states of **FA**, respectively, as well as at 10.86 and 10.63 eV to the $\tilde{B}^+\,^2A''$ state of **1ECP** and $\tilde{B}^+\,^2A'$ state of **2ECP**, respectively. There are two pronounced bands in the ms-TPES at ca. 9.2 and 10.1 eV in the low-*T* ms-TPES (see

Table 1. Calculated and Measured Adiabatic Ionization Energies to the Doublet $\tilde{X}^+$ $C_7H_6^+$ as well as Singlet $\tilde{X}^+$ and Triplet $\tilde{a}^+$ $C_7H_5^+$ Ground States

species	formula	m/z	state	CBS-QB3 (eV)	expt (eV)[a]	lit. (eV)
FA	$C_5H_4{=}C{=}CH_2$	90	$\tilde{X}^+\,^2A_2$	8.26	8.23 ± 0.01	8.22 ± 0.01[b]
1ECP	1-$C_5H_5{-}C{\equiv}CH$	90	$\tilde{X}^+\,^2A''$	8.25	8.27 ± 0.01	
2ECP	2-$C_5H_5{-}C{\equiv}CH$	90	$\tilde{X}^+\,^2A''$	8.49	8.49 ± 0.01	
5ECP	5-$C_5H_5{-}C{\equiv}CH$	90	$\tilde{X}^+\,^2A''$	8.71	8.76 ± 0.02	
FArad	$C_5H_4{-}C{\equiv}CH$	89	$\tilde{X}^+\,^1A_1$	8.31	8.20 ± 0.01	8.19 ± 0.02[b]
			$\tilde{a}^+\,^3B_2$ (and $\tilde{A}^+\,^1B_2$)	8.36	8.33 ± 0.02	

[a]Experimental ionization energies take the 0.01 eV Stark shift in the DC extraction field of the spectrometer into account.[39] [b]Steinbauer et al.[23] without Stark-correction.

https://dx.doi.org/10.1021/acs.jpca.1c00149
J. Phys. Chem. A XXXX, XXX, XXX−XXX

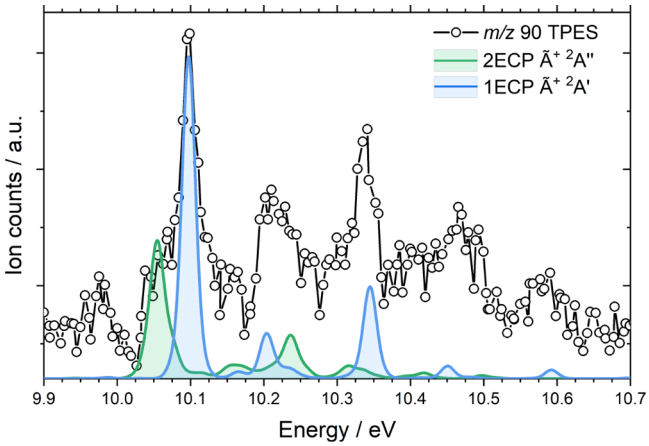

Figure 4. Mass-selected threshold photoelectron spectrum of m/z 90 upon pyrolysis of phthalide at 1166 K shown together with the Franck−Condon simulated spectra of the ionization to the first electronically excited states of **1ECP** (blue) and **2ECP** (green).

Figure S1), corresponding to the energy range of the $\tilde{A}^+$ and $\tilde{B}^+$ states of the **FA** cation, respectively. These bands lack fine structure, which suggests that they undergo significant geometry relaxation and/or are short-lived. Similar behavior was also found for fulvenone, which exhibits the same cyclopentadienyl moiety and exhibits a structureless $\tilde{A}^+$ state band.[42] $\tilde{B}^+$ states of the **1ECP** and **2ECP** cations appear to be beyond the energy range studied herein.

It is interesting to compare our m/z 90 ms-TPES (IE = 8.23 eV) with the He I photoelectron spectra of Botter et al.[22] (IE = 8.22 eV) and of Müller et al.[18] (IE = 8.29 eV). We agree with the overall assignment of Müller et al.[18] that the $\tilde{X}^+ {}^2A_2$, $\tilde{A}^+ {}^2B_1$, and $\tilde{B}^+ {}^2B_2$ states are found in the 8−11 eV energy range. However, our **FA** threshold photoelectron spectrum exhibits a strong ground-state band, followed by weak and broad peaks belonging to the excited state. In contrast, the He I spectrum shows three similarly intense bands. The m/z 90 ms-TPES of Steinbauer et al.[23] (IE = 8.22 eV) also displays a drop of signal intensity, although, based on their m/z 89 results *(vide infra)*, it appears that the signal intensity dropped at higher photon energies because of an experimental artifact. More importantly, both He I photoelectron spectra exhibit a three-membered vibronic progression in the ground-state band, where the peak heights are by and large comparable. Our **FA** TPES, on the other hand, exhibits a ground-state band structure with only two strong resonances. Furthermore, we could assign the relatively sharp peak at ca. 10.1 eV unambiguously to an isomer of **FA**, because it is completely absent in the T = 1030 K spectrum. Its presence in the He I photoelectron spectra suggests that Botter et al.[22] and Müller et al.[18] studied a mix of C_7H_6 isomers instead of a sample of pure **FA**. This is not entirely surprising, as they synthesized and separated bulk **FA** and introduced it in the spectrometer, assuming that it maintained its isomeric purity, which may not have been entirely true.

The Fulvenallenyl Radical: *m/z* 89 ms-TPES. An overview spectrum showing the ms-TPE spectra of the m/z 89 mass channel is available from the Supporting Information (Figure S2). In Figure 5, only the (low-energy) region between 8.1 and 9.0 eV (top panel) and the (high-energy) region between 10.1 and 11 eV (bottom panel) are highlighted, as this is where vibrationally resolved transitions are observed. Two

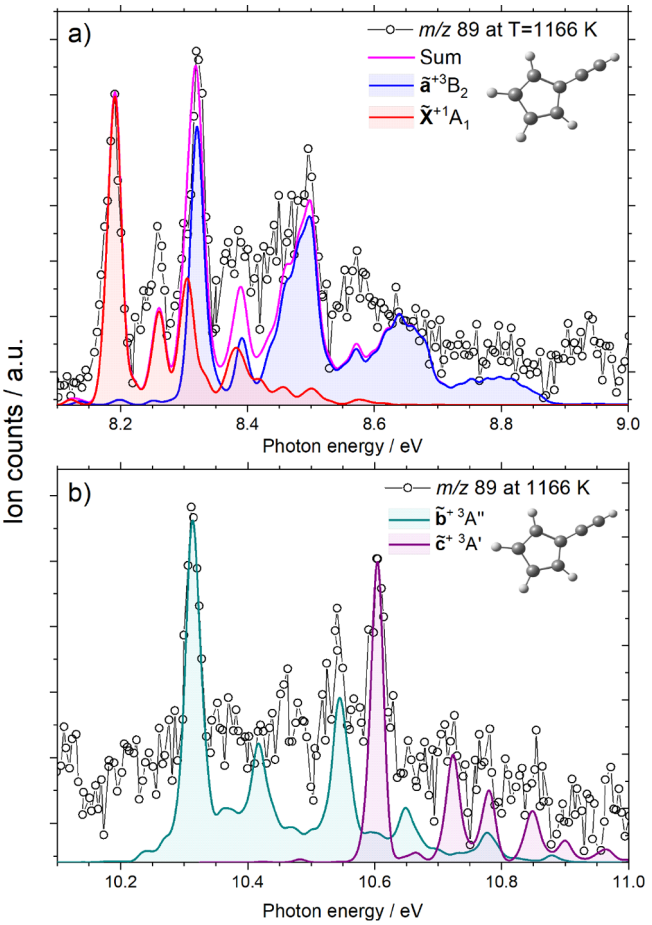

Figure 5. Threshold photoelectron spectra of (a) the C_7H_5 radical formed upon pyrolysis of fulvenallene displayed together with Franck−Condon simulations of the singlet and triplet ground states of the closed-shell fulvenallenyl radical and (b) a zoom-in of the high energy range of the C_5H_7 radical TPES shown together with Franck−Condon simulated spectra of the first ($\tilde{b}^+ {}^3A''$) and second ($\tilde{c}^+ {}^3A'$) excited triplet states.

strong and resolved resonances are seen in the low-energy part of the spectrum at 8.20 and 8.32 eV. The former was previously attributed to ionization to the ionic ground state ($^1A_1$) of the resonance-stabilized **FArad** ($C_7H_5^\bullet$).[23] Indeed, the simulated spectrum of the singlet ground state of the fulvenallenyl cation, shown in red in Figure 5, matches the first two resonances seen at 8.20 and 8.26 eV very nicely. Curiously, the second strong resonance at 8.32 eV and the strong and broad feature centered around 8.5 eV were not reported before. We believe that dropping overall sample levels or VUV flux may be a reason for the missing signal above 8.3 eV in the spectrum of Steinbauer et al.[23] This structure can only be explained if we consider the lowest-lying $\tilde{a}^+ {}^3B_2$ triplet state of the **FArad** cation, the Franck−Condon simulation of which is plotted in blue in Figure 5. We note that EOM-IP-CCSD calculations predict the first singlet excited state $\tilde{A}^+ {}^1B_2$ to be near-degenerate with the first $\tilde{a}^+$ triplet state. However, TD-DFT calculations have not converged for the $\tilde{A}^+ {}^1B_2$ state, which implies strong coupling with the $\tilde{X}^+$ state. Thus, the actual low-energy band (top panel Figure 5) may contain three contributing states.

There is vibronic structure in the 10.1−11.0 eV range of the m/z 89 ms-TPES of $C_7H_5^\bullet$, as shown in Figure 5b. Our

https://dx.doi.org/10.1021/acs.jpca.1c00149
J. Phys. Chem. A XXXX, XXX, XXX−XXX

tentative assignment, based on triplet TD-DFT frequency analysis, Franck−Condon simulations, and EOM-IP-CCSD calculations, suggests that transitions to $\tilde{\mathbf{b}}^+\,^3A''$ ($^3A_2$ in C_{2v}) and $\tilde{\mathbf{c}}^+\,^3A'$ ($^3A_1$ in C_{2v}) are seen in this energy range. Vertical ionization energies are 10.61 and 10.78 eV to these states, and adiabatic ionization energies, calculated at the EOM-IP-CCSD/cc-pVTZ level at the TD-DFT optimized C_s geometries, were found to be 10.50 and 10.67 eV, respectively. The TD-DFT energies of these states are within 30 meV of each other, but the different symmetries and geometries, as well as the EOM-IP results, confirm that two different states are at play. This part of the spectrum is, thus, best reproduced by a combined $\tilde{\mathbf{b}}^+$ and $\tilde{\mathbf{c}}^+$ triplet simulation of **FArad**, which also yields ionization energies to these states (see Table 2). The vertical ionization energy to the $\tilde{\mathbf{C}}^+\,^1A_2$ singlet state lies also in this energy range at 10.74 eV. TD-DFT geometry optimizations have failed for this state, which may indicate strong coupling with the lower-lying singlet states. This would imply a short lifetime and a broad and structureless contribution of this state to the TPES. Thus, it is likely that this state contributes only to the baseline of the ms-TPES in the 10.1−11.0 eV energy range.

Potential Energy Surface Calculations. Internal coordinate scans and constrained optimizations were carried out at the B3LYP/6-311++G(d,p) level of theory to explore the potential energy surface (PES) and rationalize the detected products. The formation of the C_7H_6 species **INT1** by CO_2-loss from phthalide, as well as the reaction steps leading to products are described in detail in the Supporting Information. Here, we only focus on the rate-limiting transition states that connect the initially formed **INT1** to the detected pyrolysis products. A summary of the PES is shown in Figure 6.

INT1 is formed by CO_2-loss from the hot phthalide precursor. Unrestricted density function theory calculations with a symmetry-broken initial guess confirm it to be an open-shell singlet (OSS) species with $\langle S^2\rangle$ = 1.02. The energy of **INT1** shown in Figure 6 is determined by applying the Ziegler−Cramer correction,[43] similarly to a recent study by Kvaskoff et al.[24] **INT1** is the only OSS singlet species in Figure 6. The lowest barrier from this intermediate is **TS1** at 231 kJ mol^{-1} leading to fulvenallene (**FA**). Alternatively, **INT1** can cross **TS13** located at 276 kJ mol^{-1} and form **5ECP**. This transition state is lower than the one found to connect **INT1** and **5ECP** in the earlier study by Kvaskoff et al.[24] Hydrogen migration over barriers **TS11** and **TS12**, located at 143 and 131 kJ mol^{-1}, respectively, result in **1ECP** and **2ECP**. The latter two products are the two most energetically stable isomers on this branch of the reaction. The fulvenallenyl radical ($C_7H_5^\bullet$ at an energy of 333 kJ mol^{-1} (shown with the dotted line in Figure 6) can form from the reaction products shown in blue on the PES via hydrogen abstraction without a reverse barrier. The PES provides valuable qualitative insights into the formation of products as a function of energy and, thus, temperature. The channel to **FA** opens up first, and the formation path to **ECP** and eventually **FArad** only opens up when the energy of the system is increased further.

Table 2. Cation Excited States and Vertical Ionization Energies together with the Experimentally Determined Band Origins

species	state	EOM-IP-CCSD (eV)	expt (eV)
FA	$\tilde{\mathbf{A}}^+\,^2B_1$	9.28	9.2[a]
	$\tilde{\mathbf{B}}^+\,^2B_2$	10.23	10.1[a]
1ECP	$\tilde{\mathbf{A}}^+\,^2A'$	10.47	10.10 ± 0.03
2ECP	$\tilde{\mathbf{A}}^+\,^2A''$	10.34	10.06 ± 0.03
FArad	$\tilde{\mathbf{b}}^+\,^3A''$	10.61	10.31 ± 0.02
	$\tilde{\mathbf{c}}^+\,^3A'$	10.78	10.60 ± 0.03

[a]Unresolved bands with no clear origin transition.

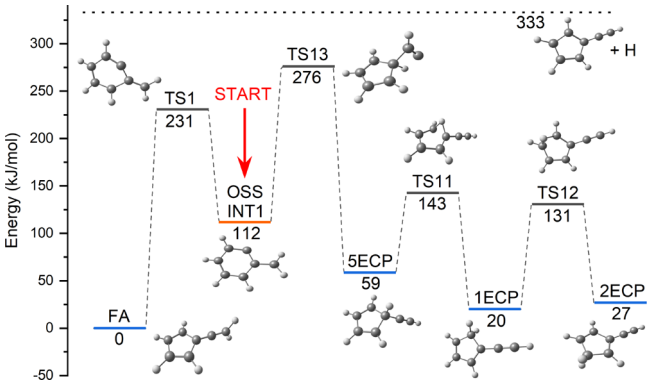

Figure 6. Summary of the C_7H_6 potential energy surface showing the rate-limiting transition states leading to the products **FA**, **5ECP**, **1ECP**, and **2ECP**. The reactant is **INT1**, formed by CO_2 loss from phthalide. Labeling of transition states is adopted from the full PES, available in the Supporting Information. The energy scale is referenced to the lowest-lying C_7H_6 product fulvenallene (**FA**). Note: direct pathways to the $C_7H_5^\bullet$ resonance-stabilized radical **FArad** (at 333 kJ mol^{-1}) through barrierless H atom abstraction are accessible from all products marked in blue.

Simplified Reactor Model. The residence time in the reactor is on the order of 100 μs, which is sufficiently long for species to rethermalize multiple times.[44] In order to establish what the thermal equilibrium in the microreactor would look like, we refined the DFT-calculated energetics in Figure 6 using the CBS-QB3 method and arrived at 0, 40, 10, 14, and 334 kJ mol^{-1} for **FA**, **5ECP**, **1ECP**, **2ECP**, and **FArad** + H, respectively. On the basis of these energies and the harmonic state functions, we calculated the Boltzmann distribution and the isomer distribution of the C_7H_6 species as a function of temperature. However, once C_7H_6 is energetic enough to lose a hydrogen atom, it may form C_7H_5 irreversibly. To account for unimolecular fragmentation, we introduce a rethermalization cycle count; in each cycle, the population of C_7H_6 species above the H-loss threshold dissociates and contributes to the C_7H_5 abundance. Assuming equal photoionization cross sections, the population of **FArad** is ca. one-third at 1160 K as observed in Figure 2. To reproduce this value, we arrived at a rethermalization cycle count of 390. If the remaining C_7H_6 population is in thermal equilibrium, the product ratios should correspond to Figure 7 as a function of reactor temperature. The model reproduces the quickly rising m/z 89 signal with rising temperature in Figure 1. However, in contrast with the large **1ECP** signal seen in Figure 3, the **ECP** species are always minor products with a plateauing abundance at ca. 1000 K, and the more stable **FA** should always dominate the spectrum. Therefore, **FA** and the **ECP** products are not in thermal equilibrium but are already disconnected below the H-loss barrier (Figure 6). Branching from **INT1** is determined by kinetic effects, and the large stabilization of the C_7H_6 products formed results in slow isomerization between **FA**, **INT1**, and the **ECP** species in the narrow energy window below the H-loss threshold. Thus, we can show that although various C_7H_6

https://dx.doi.org/10.1021/acs.jpca.1c00149
J. Phys. Chem. A XXXX, XXX, XXX−XXX

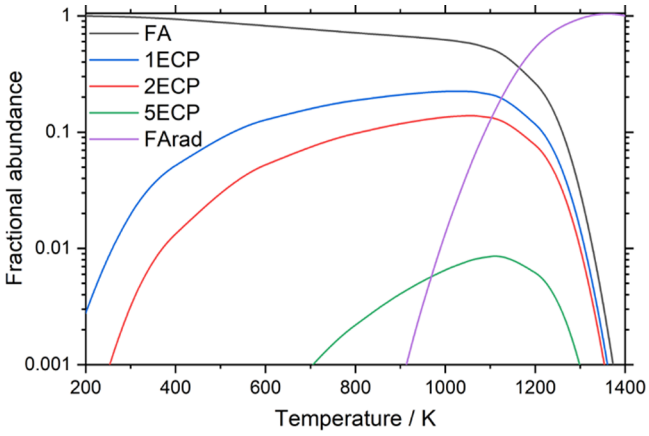

Figure 7. Predicted phthalide pyrolysis product distribution as a function of temperature assuming that C_7H_6 species above the H-loss barrier lose hydrogen irreversibly in 390 rethermalization cycles, while the remaining C_7H_6 product distribution is in thermal equilibrium.

pyrolysis products coexist in a broad temperature range and their interconversion is energetically allowed, yet the branching ratios are determined by kinetic effects and pyrolysis yields a C_7H_6 isomer distribution far from equilibrium.

CONCLUSIONS

We pyrolyzed phthalide and recorded mass spectra as a function of temperature to identify pyrolysis products at m/z 90 and 89. The experiments revealed a richer phthalide pyrolysis chemistry than previously reported. It furthermore led us to rediscover C_7H_6 isomerism, as previously unveiled by D'Amore et al.[19] Photoion mass-selected threshold photoelectron spectra of the C_7H_6 channel were used to identify the temperature-dependent contributions of the **FA** and three **ECP** isomers. The latter are newly assigned pyrolysis products of phthalide. The $C_7H_5^\bullet$ radical can be formed by H loss from any of the C_7H_6 isomers, and its photoelectron spectrum has also been recorded. Accurate ionization energies were determined for **FA**, **1ECP**, **2ECP**, and **5ECP** and were compared to computed adiabatic ionization energies. A vibrationally resolved excited-state band was detected around 10.1 eV and was attributed to the sum of the first electronically excited state of **1ECP** and **2ECP**. The ionic ground state (singlet) of the **FArad** radical was found at 8.20 eV and the triplet ground state was found to be 0.13 eV higher in energy. Furthermore, a vibrationally resolved excited-state band in the photoelectron spectrum of $C_7H_5^\bullet$ was assigned to the first and second excited triplet states. The temperature-dependent formation of the various products was rationalized by complementary quantum chemical computations. A simplified reactor model shows that irreversible hydrogen atom loss from C_7H_6 may stop the evolution of thermal equilibrium, and the branching ratio between the **FA** and **ECP** products is determined by kinetic effects instead.

Temperature-dependent ms-TPES, ground- and excited-state calculations as well as Franck−Condon models helped assign the congested ground-state band of C_7H_6 and the excited-state peaks in an isomer-selective manner. They also helped us determine the singlet and triplet state contributions to the **FArad** photoelectron spectrum. This illustrates how careful analysis of PEPICO data can contribute to an isomer-specific understanding of reaction processes as well as providing reference data for analytical purposes. Different isomers may exhibit different reactivity with respect to PAH growth, as illustrated by the dependence of ring condensation of C_7H_6 to form heptafulvalene on the reaction conditions, originally reported by D'Amore et al.[19] Thus, isomer-selective detection of elusive PAH precursor intermediates may help us understand PAH growth and soot formation in more detail.

ASSOCIATED CONTENT

Supporting Information

The Supporting Information is available free of charge at https://pubs.acs.org/doi/10.1021/acs.jpca.1c00149.

Temperature evolution of the overview spectra of the m/z 90 product and an overview TPE spectra of the m/z 89 radical product, the potential energy surface of phthalide dissociation, and the full C_7H_6 potential energy surface (PDF)

AUTHOR INFORMATION

Corresponding Author

Jordy Bouwman − *Laboratory for Astrophysics, Leiden Observatory, Leiden University, 2300 RA Leiden, The Netherlands;* orcid.org/0000-0002-3615-1703; Phone: +31(0)71 5278432; Email: bouwman@strw.leidenuniv.nl

Authors

Helgi R. Hrodmarsson − *Laboratory for Astrophysics, Leiden Observatory, Leiden University, 2300 RA Leiden, The Netherlands;* orcid.org/0000-0002-9613-5684

G. Barney Ellison − *Department of Chemistry and Biochemistry, University of Colorado Boulder, Boulder, Colorado 80309-0215, United States;* orcid.org/0000-0003-3107-1613

Andras Bodi − *Laboratory for Synchrotron Radiation and Femtochemistry, Paul Scherrer Institute, 5232 Villigen, Switzerland;* orcid.org/0000-0003-2742-1051

Patrick Hemberger − *Laboratory for Synchrotron Radiation and Femtochemistry, Paul Scherrer Institute, 5232 Villigen, Switzerland;* orcid.org/0000-0002-1251-4549

Complete contact information is available at: https://pubs.acs.org/10.1021/acs.jpca.1c00149

Notes

The authors declare no competing financial interest.

ACKNOWLEDGMENTS

J.B. acknowledges The Netherlands Organisation for Scientific Research (Nederlandse Organisatie voor Wetenschappelijk Onderzoek, NWO) for a Vidi grant (Grant Number 723.016.006) which was used to support this work. This work was carried out on the Dutch national e-infrastructure with the support of SURF Cooperative (Grant Number e-infra 46011). H.R.H. acknowledges support from the Marie Skłodowska Curie Actions, Proposal ID: 838372. The i^2PEPICO experiments were performed at the VUV beamline at the Swiss Light Source (Paul Scherrer Institute, 5232 Villigen, Switzerland). P.H. and A.B. gratefully acknowledge funding by the Swiss Federal Office of Energy (BFE Contract Number SI/501269-01). The authors are grateful to David Kvaskoff for providing valuable insights into the DFT treatment of open-shell singlet species.

https://dx.doi.org/10.1021/acs.jpca.1c00149
J. Phys. Chem. A XXXX, XXX, XXX−XXX

REFERENCES

(1) Richter, H.; Howard, J. B. Formation of polycyclic aromatic hydrocarbons and their growth to soot—a review of chemical reaction pathways. *Prog. Energy Combust. Sci.* **2000**, *26*, 565−608.

(2) Kim, K.-H.; Jahan, S. A.; Kabir, E.; Brown, R. J. A review of airborne polycyclic aromatic hydrocarbons (PAHs) and their human health effects. *Environ. Int.* **2013**, *60*, 71−80.

(3) Allamandola, L. J.; Tielens, A. G. G. M.; Barker, J. R. Polycyclic aromatic hydrocarbons and the unidentified infrared emission bands: auto exhaust along the milky way. *Astrophys. J.* **1985**, *290*, L25−L28.

(4) Allamandola, L. J.; Tielens, A. G. G. M.; Barker, J. R. Interstellar polycyclic aromatic hydrocarbons - The infrared emission bands, the excitation/emission mechanism, and the astrophysical implications. *Astrophys. J., Suppl. Ser.* **1989**, *71*, 733−775.

(5) Tielens, A. Interstellar Polycyclic Aromatic Hydrocarbon Molecules. *Annu. Rev. Astron. Astrophys.* **2008**, *46*, 289−337.

(6) Frenklach, M.; Feigelson, E. D. Formation of Polycyclic Aromatic Hydrocarbons in Circumstellar Envelopes. *Astrophys. J.* **1989**, *341*, 372.

(7) Cherchneff, I.; Barker, J. R.; Tielens, A. e. G. G. M. Polycyclic Aromatic Hydrocarbon Formation in Carbon-rich Stellar Envelopes. *Astrophys. J.* **1992**, *401*, 269.

(8) Lafleur, A. L.; Taghizadeh, K.; Howard, J. B.; Anacleto, J. F.; Quilliam, M. A. Characterization of flame-generated C_{10} to C_{160} polycyclic aromatic hydrocarbons by atmospheric-pressure chemical ionization mass spectrometry with liquid introduction via heated nebulizer interface. *J. Am. Soc. Mass Spectrom.* **1996**, *7*, 276−286.

(9) Wu, X.-Z.; Yao, Y.-R.; Chen, M.-M.; Tian, H.-R.; Xiao, J.; Xu, Y.-Y.; Lin, M.-S.; Abella, L.; Tian, C.-B.; Gao, C.-L.; et al. Formation of Curvature Subunit of Carbon in Combustion. *J. Am. Chem. Soc.* **2016**, *138*, 9629−9633.

(10) Bouwman, J.; de Haas, A. J.; Oomens, J. Spectroscopic evidence for the formation of pentalene$^+$ in the dissociative ionization of naphthalene. *Chem. Commun.* **2016**, *52*, 2636−2638.

(11) de Haas, A. J.; Oomens, J.; Bouwman, J. Facile pentagon formation in the dissociation of polyaromatics. *Phys. Chem. Chem. Phys.* **2017**, *19*, 2974−2980.

(12) Bouwman, J.; Boersma, C.; Bulak, M.; Kamer, J.; Castellanos, P.; Tielens, A. G. G. M.; Linnartz, H. Gas-phase infrared spectroscopy of the rubicene cation ($C_{26}H_{14}^+$) - A case study for interstellar pentagons. *Astron. Astrophys.* **2020**, *636*, A57.

(13) Hansen, N.; Kasper, T.; Klippenstein, S. J.; Westmoreland, P. R.; Law, M. E.; Taatjes, C. A.; Kohse-Höinghaus, K.; Wang, J.; Cool, T. A. Initial Steps of Aromatic Ring Formation in a Laminar Premixed Fuel-Rich Cyclopentene Flame. *J. Phys. Chem. A* **2007**, *111*, 4081−4092.

(14) Wong, M. W.; Wentrup, C. Interconversions of Phenylcarbene, Cycloheptatetraene, Fulvenallene, and Benzocyclopropene. A Theoretical Study of the C_7H_6 Energy Surface. *J. Org. Chem.* **1996**, *61*, 7022−7029.

(15) Rao, V. S.; Skinner, G. B. Formation of hydrogen atoms in pyrolysis of ethylbenzene behind shock waves. Rate constants for the thermal dissociation of the benzyl radical. *Symp. Combust., [Proc.]* **1988**, *21*, 809−814.

(16) Buckingham, G. T.; Porterfield, J. P.; Kostko, O.; Troy, T. P.; Ahmed, M.; Robichaud, D. J.; Nimlos, M. R.; Daily, J. W.; Ellison, G. B. The thermal decomposition of the benzyl radical in a heated microreactor. II. Pyrolysis of the tropyl radical. *J. Chem. Phys.* **2016**, *145*, 014305.

(17) da Silva, G.; Bozzelli, J. W. The C7H5 Fulvenallenyl Radical as a Combustion Intermediate: Potential New Pathways to Two- and Three-Ring PAHs. *J. Phys. Chem. A* **2009**, *113*, 12045−12048.

(18) Müller, C.; Schweig, A.; Thiel, W.; Grahn, W.; Bergman, R. G.; Vollhardt, K. P. C. Theory and application of photoelectron spectroscopy. 80. Photoelectron spectra of 2,5-dehydrotropylidene, 3,6-dehydrooxepin, and fulvenallene. *J. Am. Chem. Soc.* **1979**, *101*, 5579−5581.

(19) D'Amore, M. B.; Bergman, R. G.; Kent, M.; Hedaya, E. Pressure-dependent formation of bicyclo[3,2,0]hepta-1,4,6-triene, fulvenallene, and ethynylcyclopentadiene in the pyrolysis of 1,2-diethynylcyclopropane. *J. Chem. Soc., Chem. Commun.* **1972**, 49.

(20) Wiersum, U.; Nieuwenhuis, T. Preparative flash vacuum thermolysis. A convenient preparation of fulvenallene from phthalide. *Tetrahedron Lett.* **1973**, *14*, 2581−2584.

(21) Wentrup, C.; Müller, P. One-step syntheses of fulvene and fulvenallen: Thermolysis of α-coumaranone, phthalide, and benzocyclopropene. *Tetrahedron Lett.* **1973**, *14*, 2915−2918.

(22) Botter, R.; Jullien, J.; Pechine, J.; Piade, J.; Solgadi, D. Ionization potentials of unstable species: Photoelectron spectrum of fulvenallene. *J. Electron Spectrosc. Relat. Phenom.* **1978**, *13*, 141−143.

(23) Steinbauer, M.; Hemberger, P.; Fischer, I.; Bodi, A. Photoionization of C_7H_6 and C_7H_5: Observation of the Fulvenallenyl Radical. *ChemPhysChem* **2011**, *12*, 1795−1797.

(24) Kvaskoff, D.; Lüerssen, H.; Bednarek, P.; Wentrup, C. Phenylnitrene, Phenylcarbene, and Pyridylcarbenes. Rearrangements to Cyanocyclopentadiene and Fulvenallene. *J. Am. Chem. Soc.* **2014**, *136*, 15203−15214.

(25) Li, Y.; Zhang, L.; Tian, Z.; Yuan, T.; Wang, J.; Yang, B.; Qi, F. Experimental Study of a Fuel-Rich Premixed Toluene Flame at Low Pressure. *Energy Fuels* **2009**, *23*, 1473−1485.

(26) Bouwman, J.; Bodi, A.; Hemberger, P. Nitrogen matters: the difference between PANH and PAH formation. *Phys. Chem. Chem. Phys.* **2018**, *20*, 29910−29917.

(27) Bodi, A.; Johnson, M.; Gerber, T.; Gengeliczki, Z.; Sztáray, B.; Baer, T. Imaging photoelectron photoion coincidence spectroscopy with velocity focusing electron optics. *Rev. Sci. Instrum.* **2009**, *80*, 034101.

(28) Bodi, A.; Hemberger, P.; Gerber, T.; Sztáray, B. A new double imaging velocity focusing coincidence experiment: i^{2}PEPICO. *Rev. Sci. Instrum.* **2012**, *83*, 083105.

(29) Sztáray, B.; Voronova, K.; Torma, K. G.; Covert, K. J.; Bodi, A.; Hemberger, P.; Gerber, T.; Osborn, D. L. CRF-PEPICO: Double velocity map imaging photoelectron photoion coincidence spectroscopy for reaction kinetics studies. *J. Chem. Phys.* **2017**, *147*, 013944.

(30) Kohn, D. W.; Clauberg, H.; Chen, P. Flash pyrolysis nozzle for generation of radicals in a supersonic jet expansion. *Rev. Sci. Instrum.* **1992**, *63*, 4003−4005.

(31) Sztáray, B.; Baer, T. Suppression of hot electrons in threshold photoelectron photoion coincidence spectroscopy using velocity focusing optics. *Rev. Sci. Instrum.* **2003**, *74*, 3763−3768.

(32) Frisch, M. J.; Trucks, G. W.; Schlegel, H. B.; Scuseria, G. E.; Robb, M. A.; Cheeseman, J. R.; Scalmani, G.; Barone, V.; Petersson, G. A.; Nakatsuji, H. et al. *Gaussian 16*, Rev. A.03; Gaussian Inc.: Wallingford, CT, 2016.

(33) Shao, Y.; Molnar, L. F.; Jung, Y.; Kussmann, J.; Ochsenfeld, C.; Brown, S. T.; Gilbert, A. T. B.; Slipchenko, L. V.; Levchenko, S. V.; O'Neill, D. P.; et al. Advances in methods and algorithms in a modern quantum chemistry program package. *Phys. Chem. Chem. Phys.* **2006**, *8*, 3172−91.

(34) Montgomery, J. A.; Frisch, M. J.; Ochterski, J. W.; Petersson, G. A. A complete basis set model chemistry. VII. Use of the minimum population localization method. *J. Chem. Phys.* **2000**, *112*, 6532−6542.

(35) Stanton, J. F.; Gauss, J. Analytic energy derivatives for ionized states described by the equation-of-motion coupled cluster method. *J. Chem. Phys.* **1994**, *101*, 8938.

(36) Mozhayskiy, A.; Krylov, A. *ezSpectrum*, Ver. 3.0.

(37) Linstrom, P.; Mallard, E. W.G. *NIST Chemistry WebBook: NIST Standard Reference Database Number 69*; National Institute of Standards and Technology: Gaithersburg, MD, 2020.

(38) Yu, T.; Wu, X.; Zhou, X.; Bodi, A.; Hemberger, P. Hydrogen migration as a potential driving force in the thermal decomposition of dimethoxymethane: New insights from pyrolysis imaging photoelectron photoion coincidence spectroscopy and computations. *Combust. Flame* **2020**, *222*, 123−132.

(39) Bodi, A.; Shuman, N.; Baer, T. On the ionization and dissociative photoionization of iodomethane: A definitive exper-

https://dx.doi.org/10.1021/acs.jpca.1c00149
J. Phys. Chem. A XXXX, XXX, XXX−XXX

imental enthalpy of formation of CH_3I. *Phys. Chem. Chem. Phys.* **2009**, *11*, 11013.
(40) Bierkandt, T.; Hemberger, P.; Oßwald, P.; Köhler, M.; Kasper, T. Insights in m-xylene decomposition under fuel-rich conditions by imaging photoelectron photoion coincidence spectroscopy. *Proc. Combust. Inst.* **2017**, *36*, 1223−1232.
(41) Reusch, E.; Holzmeier, F.; Gerlach, M.; Fischer, I.; Hemberger, P. Decomposition of Picolyl Radicals at High Temperature: A Mass Selective Threshold Photoelectron Spectroscopy Study. *Chem. - Eur. J.* **2019**, *25*, 16652−16659.
(42) Hemberger, P.; Pan, Z.; Bodi, A.; van Bokhoven, J. A.; Ormond, T. K.; Ellison, G. B.; Genossar, N.; Baraban, J. H. The Threshold Photoelectron Spectrum of Fulvenone: A Reactive Ketene Derivative in Lignin Valorization. *ChemPhysChem* **2020**, *21*, 2217−2222.
(43) Johnson, W. T. G.; Sullivan, M. B.; Cramer, C. J. meta and para substitution effects on the electronic state energies and ring-expansion reactivities of phenylnitrenes. *Int. J. Quantum Chem.* **2001**, *85*, 492−508.
(44) Guan, Q.; Urness, K. N.; Ormond, T. K.; David, D. E.; Barney Ellison, G.; Daily, J. W. The properties of a micro-reactor for the study of the unimolecular decomposition of large molecules. *Int. Rev. Phys. Chem.* **2014**, *33*, 447−487.

https://dx.doi.org/10.1021/acs.jpca.1c00149
J. Phys. Chem. A XXXX, XXX, XXX−XXX